4. Takahashi, S., Katagiri, T., Shinozaki, K. Y. and Shinozaki, K., An *Arabidopsis* gene encoding a Ca^{2+} binding protein is induced by abscisic acid during dehydration. *Plant Cell Physiol.*, 2000, **41**(7), 898–903.
5. Kim, M. C., Chung, W. S., Yun, D. J. and Cho, M. J., Calcium and calmodulin-mediated regulation of gene expression in plants. *Mol. Plant*, 2009, **2**, 13–21.
6. Feng, J., Li, J., Liu, H., Gao, Q., Duan, K. and Zou, Z., Isolation and characterization of a calcium-dependent protein kinase gene, *FvCDPK1*, responsive to abiotic stress in woodland strawberry (*Fragaria vesca*). *Plant Mol. Biol. Rep.*, 2013, **31**, 443–456.
7. Wang, T. Z., Zhang, J. L., Tian, Q. Y., Zhao, M. G. and Zhang, W. H., A *Medicago truncatula* EF-hand family gene, *MtCaMP1*, is involved in drought and salt stress tolerance. *PLoS One*, 2013, **8**(4), e58952.
8. Loukehaich, R. *et al.*, SpUSP, an annexin-interacting universal stress protein, enhances drought tolerance in tomato. *J. Exp. Bot.*, 2012, **63**, 5593–5606.
9. Polge, C. and Thomas, M., SNF1/AMPK/SnRK1 kinases, global regulators at the heart of energy control? *Trends Plant Sci.*, 2007, **12**, 20–28.
10. Fowler, T. J., Bernhardt, C. and Tierney, M. L., Characterization and expression of four proline-rich cell wall protein genes in *Arabidopsis* encoding two distinct subsets of multiple domain proteins. *Plant Physiol.*, 1999, **121**, 1081–1091.
11. He, C. Y., Zhang, J. S. and Chen, S. Y., A soybean gene encoding a proline-rich protein is regulated by salicylic acid, an endogenous circadian rhythm and by various stresses. *Theor. Appl. Genet.*, 2002, **104**, 1125–1131.
12. Gothandam, K. M., Nalini, E., Karthikeyan, S. and Shin, J. S., OsPRP3, a flower specific proline-rich protein of rice, determines extracellular matrix structure of floral organs and its overexpression confers cold-tolerance. *Plant Mol. Biol.*, 2010, **72**, 125–135.
13. Zhan, X., Wang, B., Li, H., Liu, R., Kalia, R. K., Zhu, J. K. and Chinnusamy, V., *Arabidopsis* proline-rich protein important for development and abiotic stress tolerance is involved in microRNA biogenesis. *Proc. Natl. Acad. Sci. USA*, 2012, **109**, 18198–18203.
14. Qin, L. X. *et al.*, Cotton *GhHyPRP3* encoding a hybrid proline-rich protein is stress inducible and its overexpression in *Arabidopsis* enhances germination under cold temperature and high salinity stress conditions. *Acta Physiol. Plant.*, 2013, **35**, 1531–1542.
15. Yoshida, Y., Noshiro, M., Aoyama, Y., Kawamoto, T., Horiuchi, T. and Gotoh, O., Structural and evolutionary studies on sterol 14a-demethylase P450 (CYP51), the most conserved P450 monooxygenase: II. Evolutionary analysis of protein and gene structures. *J. Biochem.*, 1997, **122**, 1122–1128.
16. Clouse, S. D. and Sasse, J. M., Brassinosteroids: essential regulators of plant growth and development. *Annu. Rev. Plant Physiol. Plant Mol. Biol.*, 1998, **49**, 427–451.
17. Kim, H. B. *et al.*, *Arabidopsis cyp51* mutant shows postembryonic seedling lethality associated with lack of membrane integrity. *Plant Physiol.*, 2005, **138**, 2033–2047.
18. Hass, G. M., Nau, H., Biemann, K., Grahn, D. T., Ericsson, L. H. and Neurath, H., The amino acid sequence of a carboxypeptidase inhibitor from potatoes. *Biochemistry*, 1975, **14**(6), 1334–1342.
19. Brick, D. J. *et al.*, A new family of lipolytic plant enzymes with members in rice, *Arabidopsis*, and maize. *FEBS Lett.*, 1995, **377**, 475–480.
20. Jakab, G., Manrique, A., Zimmerli, L., Métraux, J. P. and Mauchi-Mani, B., Molecular characterization of a novel lipase-like pathogen-inducible gene family of *Arabidopsis*. *Plant Physiol.*, 2003, **132**, 2230–2239.
21. Narusaka, Y. *et al.*, Expression profiles of *Arabidopsis* phospholipase A IIA gene in response to biotic and abiotic stresses. *Plant Cell Physiol.*, 2003, **44**, 1247–1252.
22. Lo, M., Taylor, C., Wang, L., Nowack, L., Wang, T. W. and Thompson, J., Characterization of an ultraviolet B-induced lipase in *Arabidopsis*. *Plant Physiol.*, 2004, **135**, 947–958.
23. Livak, K. J. and Schmittgen, T. D., Analysis of relative gene expression data using real time quantitative PCR and the $2^{-\Delta\Delta C(T)}$ method. *Methods*, 2001, **25**, 402–408.
24. Isokpehi, R. D., Simmons, S. S., Cohly, H. H., Ekunwe, S. I., Begonia, G. B. and Ayensu, W. K., Identification of drought-responsive universal stress proteins in viridiplantae. *Bioinf. Biol. Insights*, 2011, **5**, 41–58.
25. Bradford, K. J., Downie, A. B., Gee, O. H., Alvarado, V., Yang, H. and Dahal, P., Abscisic acid and gibberellin differentially regulate expression of genes of the SNF1-related kinase complex in tomato seeds. *Plant Physiol.*, 2003, **132**, 1560–1576.
26. Martineau, B., McBride, K. E. and Houck, C. M., Regulation of metallocarboxypeptidase inhibitor gene expression in tomato. *Mol. Gen. Genet.*, 1991, **228**(1–2), 281–286.

ACKNOWLEDGEMENTS. We thank Dr P. S. Naik, Dr Shailesh Tiwari, Dr H. C. Prasanna and Dr Suresh Reddy (Indian Institute of Vegetable Research (IIVR), Varanasi) and Dr Sanjeev Kumar (Indian Institute of Sugarcane Research, Lucknow) for useful comments and suggestions. Financial assistance for this work was provided by IIVR, Varanasi.

Received 21 December 2013; revised accepted 6 June 2014

Increase in agricultural patch contiguity over the past three decades in Ganga River Basin, India

M. D. Behera[1,*], N. Patidar[2], V. S. Chitale[1], N. Behera[2], D. Gupta[2], S. Matin[1], V. Tare[3], S. N. Panda[2] and D. J. Sen[4]

[1]Spatial Analysis and Modelling Laboratory, Centre for Oceans, Rivers, Atmosphere and Land Sciences,
[2]School of Water Resources, Department of Civil Engineering, Indian Institute of Technology Kharagpur, Kharagpur 721 302, India
[3]Department of Civil Engineering, Indian Institute of Technology Kanpur, Kanpur 208 016, India
[4]Department of Civil Engineering, Indian Institute of Technology Kharagpur, Kharagpur 721 302, India

Ganga River Basin (GRB) is the second most populous river basin in the world, which has been undergoing rapid land-use change during the last few decades. Here, we analyse the landscape dynamics in Indian GRB (IGRB) using three indices, i.e. class area, mean patch size and number of patches for 14 land-use and land-cover (LULC) classes using multi-temporal Landsat satellite datasets of 1975 and 2010. Major change was observed with the expansion of agricultural lands and human settlements and depletion of

*For correspondence. (e-mail: mdbehera@coral.iitkgp.ernet.in)

forests. Agricultural lands covered the highest area (>75%), where low to medium-sized patches have increased and patches with larger size have been slightly reduced in size over past decades. The highest increase in percentage of built-up land has been appropriately captured on medium-resolution satellite imageries using visual interpretation technique. Degradation and loss of forest areas were reported in terms of landscape indices; however, the increase of plantation is a positive sign in the basin. In general, we observed aggregation of agricultural patches and reduction of forest patches in small to medium patch sizes. We argue the utility of 'onscreen visual interpretation' technique in favour of LULC mapping to achieve absolute accuracy in such a heterogeneous landscape, as it incorporates interpreter's knowledge. We appreciate the free availability of Landsat imageries having very good radiometry that has opened the doors for exercises with minimum cost. Located in one of the most fertile regions of India, the basin accommodates more than 400 million human population. This has led to expansion of agriculture and built-up land at the cost of forest and other land covers. Understanding landscape dynamics could help in designing an effective land-use policy for IGRB.

Keywords: Agricultural patch, landsat, landscape dynamics, land use change, visual interpretation.

LANDSCAPES are geographic areas demarcated by interacting ecosystems and human interference within them[1]. Landscape ecology attempts to understand the relationships between spatial pattern and ecological processes at landscape level, which could explain the association between landscape structure, function and dynamics over time[2]. Landscape structure demonstrates the configuration of a landscape that affects ecological processes independently and interactively[3]. Landscape change is particularly observed through habitat loss, land transformation and fragmentation. Majority of the Earth's terrestrial ecosystems have been converted either to a managed forest and agriculture or to human settlements to cater to the basic needs of human beings such as food, fuel and shelter[4]. Agriculture is expanding across a variety of tropical ecosystems; however, its impacts on forests are among the most serious from an environmental perspective[5]. Globally tropical forests once spanned over 17 million sq. km, which has now declined to a mere ~11 million sq. km. It has been predicted that as tropical nations develop economically and become increasingly urbanized, they might experience drastic land-use transitions, with greater expansion of agricultural lands[6]. Forest plantations in the developing countries have increased by ~5000 sq. km/yr between 1990 and 2005, with the largest increase in China and India. Globally, India ranks second in terms of total land area under plantation, by planting non-native tree species to provide timber, fuel wood and also as a source of income through the sale of carbon credits under the Clean Development Mechanism[7]. An effective land-use policy is the need of the hour, particularly in the developing countries, which could put control on the over-increasing urbanization and agricultural expansion on the cost of other land-cover classes.

Analysis of landscape dynamics can provide crucial information to planners and researchers about landscape functions. Patch dynamics can be utilized to understand how urbanization affects landscape structure[8]. Few studies have highlighted the advantages of utilizing spatial indices to understand the drivers and pattern, composition and configuration of landscape dynamics using various landscape indices in the past decades[9,10]. Generally landscape dynamics has been analysed using spatial indices such as area of land-use or land-cover (LULC) class, number of patches and mean patch size, which could be derived at multi-temporal scale to understand the structural changes in the landscape configuration[11]. Class area denotes the sum of areas of all patches belonging to a given LULC class. Number of patches gives a count of all the patches within a class or from the entire landscape. Mean patch size is considered to be a primary predictor of heterogeneity within a given class.

Regional land-use pattern depicts interaction between humans and the environment and the influence of resources based on the basic economic activities of man. Remote sensing with multi-temporal high-resolution satellite data has become a powerful tool to effectively monitor a variety of aspects of landscape dynamics such as urban sprawl, vegetation cover change, forest degradation and most commonly various types of LULC changes[12,13]. Prior to use in land-cover classification, radiometric correction of satellite data is important, which addresses errors that arise due to both a sensor system detector error and an environmental attenuation error and affect the brightness value of pixels (e.g. changes in scene illumination, atmospheric conditions and viewing geometry)[14]. Roy *et al.*[15] found visual interpretation technique to be advantageous over digital interpretation techniques using Landsat data in forest mapping in Arunachal Pradesh. Humans are exceptionally adept at visually recognizing and interpreting complex spatial patterns and can comprehensively use shape, size, colour and texture in interpretations. Visual interpretation also allows the user to demarcate realistic objects, such as patches with irregular shapes. Therefore, unlike pixel-based or object-based approaches, visual interpretation integrates ecological knowledge into image analysis, thus making the results more ecologically meaningful[1,16]. In a recent study using visual interpretation, Chitale *et al.*[17] characterized nine communities of *Shorea robusta* in the terai landscape of Uttar Pradesh, based on moderate resolution (LISS-III) satellite data. Although visual interpretation is a time-extensive exercise, it has been widely applied in most of land-use studies in India to tackle extremely heterogeneous land mosaic without compromising on classification accuracy. In the present study, we attempt to understand the landscape dynamics in the Ganga River Basin (GRB) over the Indian territory using landscape indices based on the multi-temporal Landsat satellite datasets of 1975 and 2010.

The Indian GRB (IGRB) extends from 21°40′39″ to 31°27′39″N latitude and 73°13′00″ to 89°09′53″E longitude (Figure 1), forming a part of the composite of Ganges–Brahmaputra–Meghna basin draining 1,086,000 sq. km in Tibet, Nepal, India and Bangladesh. Flowing across the great alluvial Indo-Gangetic plains, the river Ganga is bordered by the Himalayas to the north and the Vindhya-Satpura ranges to the south. The climate varies from arid to humid; the basin extends from desert in the west to sea coast in the east and up to the Himalayan range in the north. Annual average precipitation varies from 543 mm at the western end of the basin to more than 2000 mm at the northeastern end; while average annual temperature varies from –5°C to 27°C from the north to southern and eastern parts of the basin. Ganga has significant economic, environmental and cultural value in India; hence this stimulated us to study the patterns of landscape dynamics in IGRB. It is located in north India, which accounts for 26% of its land mass, 30% of its water resources and more than 40% of its population[18]. The IGRB covers an area of 804,671 sq. km and is the largest river basin in India and the second most populous river basin of the world. Social and economic development, including agricultural land expansion has replaced most of the original natural vegetation in the IGRB. More than 95% of the upper Gangetic plain has been degraded or converted to either agriculture or urban areas[19].

Figure 1. Location of Ganga River Basin, India.

Landsat multispectral scanner (MSS) and Landsat thematic mapper (TM) satellite datasets of 1975 and 2010 respectively, were utilized to classify the landscape of IGRB into 14 LULC classes using a pre-designed classification scheme (Table 1). In all, 57 scenes of Landsat MSS and 51 scenes of Landsat TM from each season, i.e. pre-monsoon (March to May) and post-monsoon (October to December) were used to address the temporal variation in forest vegetation, agriculture and water bodies. A total of 114 scenes of Landsat MSS and 102 scenes of Landsat TM were downloaded from the United States Geological Survey (USGS) portal and first corrected for radiometry using image enhancement techniques followed by geometric correction using 'image to image geometric correction' technique to match the extent of satellite data of 1975 and 2010. Visual interpretation-based land-use and land-cover classification was done using individual scenes of satellite datasets to avoid errors due to variations in the radiometry, which arise due to mosaicking of satellite scenes. More than 250,000 polygons were manually digitized in a GIS environment ArcMap 9.3, and converted to raster layer for analysing the landscape dynamics in IGRB. Interpretation of the features through mapping was verified from high-resolution images using Google Earth and 366 ground truthing points acquired using global positioning system (GPS; Tables 2 and 3). The overall accuracy and kappa statistics were used to assess the classification accuracy. A suitable classification scheme was formulated (Table 1) keeping land cover, land use, topography, spatial and spectral resolution and purpose of mapping in mind. Present scenario of LULC (2010) was generated first, since it was appropriate to verify the interpretation of features from other available sources. LULC map of 2010 was used as reference to generate the historical scenario of 1975. Using 'support vector method', the change map was derived between 1975 and 2010 LULC and the change matrix was calculated (Figure 2, Tables 4 and 5).

Table 1. Land-use and land-cover classification scheme utilized to classify the landscape into 14 classes using Landsat MSS and Landsat TM satellite data of 1975 and 2010 respectively

Forest
Deciduous forest (DDF)
Evergreen broadleaved forest (EBF)
Evergreen needle-leaved forest (ENF)
Mixed forest (MF)
Degraded forest (DEG)
Mangroves (MG)
Non-forest
Agricultural land (AG)
Built-up land (BU)
Grassland (GL)
Scrubland (SL)
Plantation (PL)
Water body (WB)
Wasteland (WL)
Snow and ice (SI)

Table 2. Error matrix of accuracy assessment of land use (LU) and land cover (LC) map for 1975

LULC class	AG	DDF	MF	ENF	EBF	MG	DEG	PL	SL	GL	WL	WB	BU	SI	Row total	User's accuracy (%)	Kc
AG	192								2		1				195	98.46	0.9
DDF		36					1		1						38	94.74	0.9
MF			9					1							10	90.00	0.8
ENF				10	1										11	90.91	0.8
EBF					9			1							10	90.00	1
MG						10									10	100.00	1
DEG							9				1				10	90.00	0.8
PL			1		1			10							12	83.33	0.9
SL		2							13						15	86.67	0.8
GL										10	1				11	90.91	0.8
WL										1	13				14	88.89	0.8
WB												10			10	100.00	1
BU													10		10	100.00	1
SI														10	10	83.33	0.8
Column total	192	38	10	10	11	10	10	12	16	11	16	10	10	10			
Producer's accuracy (%)	100	95	90	100	82	100	90	83	81	91	81	100	100	100			
Overall classification accuracy = 91.5%																	
Overall Kappa coefficient = 0.87																	

Table 3. Error matrix of accuracy assessment of land use and land cover map for 2010

LULC class	AG	DDF	MF	ENF	EBF	MG	DEG	PL	SL	GL	WL	WB	BU	SI	Row total	User's accuracy (%)	Kc
AG	192										1				193	99.48	0.9
DDF		36							1						37	97.30	0.9
MF			10					0							10	100.00	0.9
ENF				10	1										11	90.91	0.9
EBF					9		1								10	90.00	1
MG						10									10	100.00	1
DEG							9		1						10	90.00	1
PL					1			12							13	92.31	0.9
SL		2							14	1					17	82.35	0.7
GL										9	1				10	90.00	0.8
WL										1	14				15	93.33	0.8
WB												10			10	100.00	1
BU													10		10	100.00	1
SI														10	10	100.00	0.8
Column total	192	38	10	10	11	10	10	12	16	11	16	10	10	10			
Producer's accuracy (%)	100	95	100	100	82	100	90	100	88	82	88	100	100	100			
Overall classification accuracy = 94.03%																	
Overall kappa coefficient = 0.90																	

The landscape dynamics in IGRB was studied using three spatial indices, i.e. class area (CA), number of patches (NP) and mean patch size (MP). Class area is the sum of areas (sq. km) of all patches belonging to a given class. It was calculated by computing the area occupied by a particular LULC class. Number of patches is the count of all patches within a class or across the entire landscape. A larger landscape has greater probability of finding more number of patches. Jointly, CA and NP help reveal landscape dynamics. Mean patch size acts as

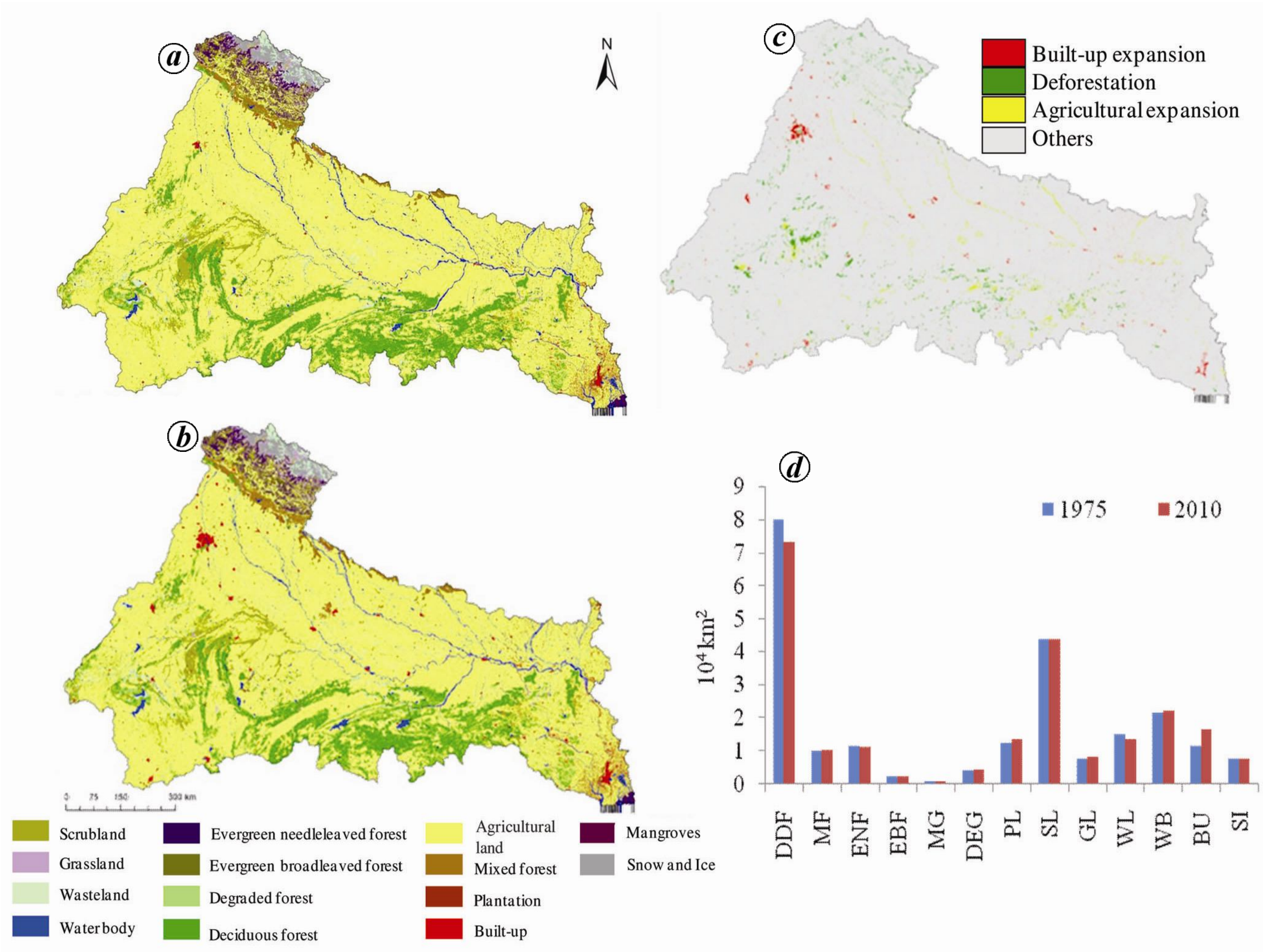

Figure 2. Land-use and land-cover maps of (***a***) 1975, (***b***) 2010, (***c***) LULC change and (***d***) area statistics (agricultural land occupied 575,937 sq. km in 1975 and 577,301 sq. km in 2010, excluded from the graph for display purpose).

Table 4. Land-use and land-cover change statistics of 1975 and 2010

	Area				Change	
	1975		2010			
Class	(sq. km)	(%)	(sq. km)	(%)	(sq. km)	(%)
AG	573,055.15	73.10	575,727.88	73.44	–2,672.73	–0.47
BU	11,286.18	1.44	16,367.98	2.09	–5,081.80	–45.03
DDF	79,252.15	10.11	73,583.62	9.39	5,668.53	7.15
DEG	4,187.94	0.53	4,768.33	0.61	–580.39	–13.86
FP	12,402.18	1.58	13,959.69	1.78	–1,557.51	–12.56
GL	7,196.65	0.92	7,028.91	0.90	167.73	2.33
MF	10,037.86	1.28	9,796.74	1.25	241.12	2.40
SI	7,374.38	0.94	7,355.97	0.94	18.41	0.25
SL	37,755.36	4.82	36,071.11	4.60	1,684.25	4.46
WB	14,375.59	1.83	12,948.21	1.65	1,427.38	9.93
WL	14,967.82	1.91	13,448.53	1.72	1,519.29	10.15
ENF	9,077.62	1.16	9,919.22	1.27	–841.60	–9.27
MG	866.08	0.11	847.58	0.11	18.50	2.14
EBF	2,115.23	0.27	508.42	0.06	1,606.81	75.96
Total	783,950.19 sq. km					

Table 5. Land-use and land-cover change matrix showing transformation of the classes in (sq. km) during 1975 and 2010 (areas <10 sq. km are not shown)

	2010													
	AG	DDF	MF	ENF	EBF	MG	DEG	PL	SL	GL	WL	WB	BU	SI
1975														
AG	565,536	159	21	–	–	–	22	970	439	213	402	3805	4369	–
DDF	2,617	72,247	513	–	–	–	945	191	3087	116	168	127	25	–
MF	274	47	9,549	–	–	–	–	175	42	11	–	49	–	–
ENF	34	32	21	10,055	126	–	–	–	888	312	25	–	–	–
EBF	–	–	–	139	2,225	–	–	–	74	–	–	–	–	–
MG	22	–	–	–	–	846	–	–	–	–	–	–	–	–
DEG	124	55	–	–	–	–	3,398	11	503	–	101	–	–	–
PL	33	16	30	–	–	–	–	11,712	70	–	–	–	450	–
SL	2,993	610	18	593	95	–	35	340	37,861	373	575	58	102	–
GL	93	34	64	445	–	–	–	15	206	6707	143	25	–	–
WL	2,310	23	–	–	–	–	–	65	349	19	12,156	129	86	–
WB	3,181	–	16	–	–	–	–	19	55	416	13	17,836	63	–
BU	78	–	–	–	–	–	–	–	–	–	–	11	11,298	–
SI	–	–	–	–	–	–	–	–	–	–	–	–	–	7,611

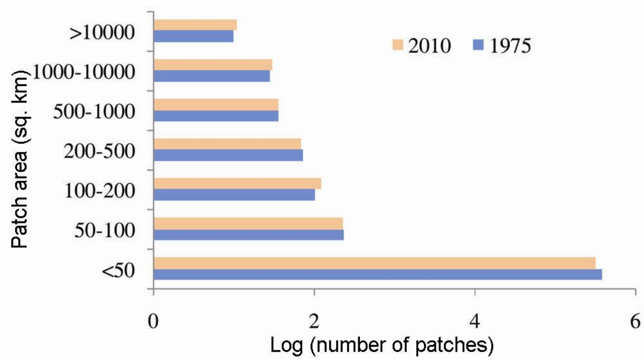

Figure 3. Patch dynamics during 1975 and 2010.

primary predictor of heterogeneity within a land-use class. In order to quantify the changes in spatial and temporal patterns within IGRB, landscape dynamics was calculated for 1975 and 2010 using LULC maps of both time-periods using Erdas Imagine 9.2 software. The landscape patches from each LULC class were divided into seven categories according to patch size range.

The landscape dynamics was studied for 14 LULC classes in IGRB for 1975 and 2010 with >90% overall classification accuracy (Tables 2 and 3). During 1975, highest class area was observed for agricultural land extending over 73.10% area, followed by dry deciduous forest covering 10.11%, scrubland with 4.82%, wasteland covering 1.91%, water body 1.83%, plantations covering 1.58% and built-up land covering 1.44% (Figure 2 *a* and *b*, Table 4). During 2010, compared to 1975, we observed increase in area under agricultural land, plantations and built-up land; decrease in area under dry deciduous forest, scrubland, wasteland, water body was also observed. In 2010, agricultural land occupied 73.44%, deciduous forest 9.39%, scrubland 4.60%, water body 1.65% and build-up land 2.09% of the area followed by other classes (Figure 2 *d*; Table 4). The agricultural land, deciduous forest, mixed forest, plantations, scrubland, grassland, wetland, water body and built-up land have undergone major transformation in the past three and half decades (Table 5).

Patch size of >10,000 sq. km area was found to be the highest in all LULC classes in IGRB, while patch size of <50 sq. km was the smallest with SD of 3.02, median of 0.05, and mode of 0.01, which indicates fragmented landscape (Figure 3 and Table 6). The number of patches with highest area in agricultural land was observed to increase from 9 to 10 during 1975 to 2010, which could be attributed to expansion of agricultural land to cater to the over-increasing demand for food. Single patch of >10,000 sq. km was observed in deciduous forest in 1975 and 2010. The highest patch size in LULC classes such as mixed forest, evergreen needle-leaved forest, scrubland, water body, and snow and ice was 1000–10,000 sq. km, while that in evergreen broadleaved forest, mangroves, degraded forest, plantation, grassland, wetland, and built-up land was 500–1000 sq. km, which indicates smaller geographical expanse of these classes. The number of patches of <50 sq. km was observed to be the highest in built-up land in 1975, with mean patch size of 0.15 sq. km with SD of 0.55, median of 0.08 and $n = 72,722$, which increased to 74,722 by 2010 with mean patch size of 0.17 sq. km with SD of 0.89 and median of 0.08. This could be attributed to intensive urbanization in IGRB, where 4369 sq. km geographical area was converted from agricultural land to built-up land during 1975 to 2010 (Tables 4 and 5). Patches of <50 sq. km were also prevalent in scrubland and plantations, where mean patch size ranged from 0.23 to 0.64 sq. km with highest number of patches of 0.01 sq. km. The scrubland was predominantly distributed along the western parts of the basin, where the climate remains dry and hot throughout the

Table 6. Land use and land cover class-wise matrices of patch dynamics of 1975 and 2010

		1975					2010				
LULC class	Class range (sq. km)	Number of polygons	Mean patch size	SD	Median	Mode	Number of polygons	Mean patch size	SD	Median	Mode
AG											
	<50	23,311	0.76	3.02	0.05	0.01	22,830	0.82	3.15	0.01	0.01
	50–100	50	68.36	12.06	66.90		47	70.61	13.42	70.50	
	100–200	27	136.88	30.18	133.81		32	139.85	31.60	130.16	
	200–500	25	318.17	88.02	295.39		24	317.05	83.18	305.30	
	500–1000	17	674.46	119.47	661.66		14	675.22	100.53	662.87	
	1000–10,000	9	3,243.99	2,139.58	2,238.45		11	2,927.69	2127.63	2073.58	
	>10,000	9	55,835.43	40,707.92	41,410.40		10	50,146.2	40,397.53	36,861.76	
DDF											
	<50	20,337	0.65	3.03	0.02	0.01	10,221	1.22	4.10	0.10	0.01
	50–100	43	71.25	13.59	71.36		44	68.71	13.65	65.65	
	100–200	19	145.73	33.95	141.10		25	148.81	28.56	149.80	
	200–500	18	329.90	91.92	315.95		16	322.48	88.42	307.49	
	500–1000	6	742.36	142.03	754.64		8	736.91	181.68	792.69	
	1000–10,000	9	2,932.52	2,250.30	1,930.47		9	2,402.34	1,406.47	2,221.78	
	>10,000	1	24,222.78				1	21,322.3			
MF											
	<50	6,288	0.29	1.98	0.02	0.01	3,279	0.46	2.68	0.03	0.01
	50–100	7	59.45	6.51	56.18		8	65.12	13.67	61.68	
	100–200	7	108.61	4.59	110.12		7	119.64	18.90	113.49	
	200–500	6	292.05	89.13	260.73		5	317.71	125.73	291.61	
	500–1000	5	719.38	76.18	693.92		5	749.87	143.31	735.58	
	1000–10,000	1	1,833.71				1	2,032.89			
ENF											
	<50	37,913	0.13	1.15	0.01	0.01	25,423	0.21	1.55	0.02	0.01
	50–100	20	70.81	14.50	72.23	86.89	9	66.39	9.78	64.36	
	100–200	6	149.81	40.14	153.72		8	158.90	31.08	164.81	
	200–500	1	493.56				1	366.52			
	500–1000	2	831.52	164.43	831.51		2	694.60	261.06	694.59	
	1000–10,000	2	1,037.80	16.16	1037.79		2	1,163.44	102.99	1163.44	
EBF											
	<50	20,688	0.10	0.81	0.01	0.01	12,629	0.16	1.13	0.03	0.01
	50–100	1	63.16				1	67.36			
	100–200	2	188.48	9.63	188.48		1	184.49			
	200–500						1	202.11			
MG											
	<50	103	3.54	7.59	0.71	0.01	104	3.27	7.31	0.66	0.01
	50–100	4	85.74	13.21	88.36		4	85.74	13.21	88.36	
	100–200	1	163.68				1	163.68			
DEG											
	<50	3,009	1.07	2.61	0.26	0.00	2,706	1.26	3.06	0.31	0.00
	50–100	2	84.27	12.63	84.26		2	56.11	8.46	56.11	
	100–200	2	111.82	16.41	111.81		2	126.09	3.77	126.09	
	200–500	2	290.46	57.27	290.45		2	322.23	15.52	322.23	
PL											
	<50	45,515	0.23	1.02	0.07	0.01	44,959	0.26	1.08	0.08	0.01
	50–100	2	76.96	8.75	76.96		3	81.94	9.67	87.30	
	100–200	2	154.74	38.41	154.73		3	135.56	18.24	127.57	
	200–500	2	322.20	42.53	322.19		4	278.13	74.28	273.92	
	500–1000	1	806.16								

(*Contd*)

Table 6. (*Contd*)

LULC class	Class range (sq. km)	1975 Number of polygons	1975 Mean patch size	1975 SD	1975 Median	1975 Mode	2010 Number of polygons	2010 Mean patch size	2010 SD	2010 Median	2010 Mode
SL											
	<50	59,671	0.46	2.33	0.02	0.01	43,699	0.64	2.70	0.04	0.01
	50–100	60	69.18	14.07	64.93	52.28	53	70.39	15.14	66.56	52.28
	100–200	18	135.21	29.31	124.93		20	137.55	33.64	125.71	
	200–500	8	270.35	65.45	241.92		7	274.38	61.60	241.99	
	500–1000	2	580.01	54.47	580.00		3	563.40	40.36	540.69	
	1000–10,000	3	2,002.10	624.11	1,992.00		3	1,890.02	757.57	1,910.87	
GL											
	<50	28,300	0.18	1.33	0.01	0.01	9,459	0.59	2.41	0.03	0.01
	50–100	17	69.55	13.98	69.75		17	77.40	13.74	80.06	
	100–200	4	138.02	39.76	133.92		4	115.63	16.84	109.56	
	200–500	1	269.01				1	270.40			
	500–1000	1	515.53				1	532.26			
WL											
	<50	30,100	0.37	1.62	0.05	0.01	26,934	0.38	1.60	0.06	0.01
	50–100	19	68.87	13.81	64.90		16	68.63	11.84	65.53	
	100–200	8	138.25	29.58	128.74		9	133.37	29.21	121.39	
	200–500	5	316.22	110.08	306.79		4	288.78	124.93	239.44	
WB											
	<50	38,036	0.22	1.24	0.03	0.01	39,749	0.22	1.27	0.04	0.01
	50–100	6	60.23	8.59	57.05		8	65.22	15.78	58.73	
	100–200	4	139.23	29.78	140.29		5	126.31	26.56	120.29	
	200–500	4	320.40	61.01	306.67		4	319.95	81.30	336.37	
	500–1000	2	895.44	40.67	895.44		1	888.69			
	1000–10,000	1	9,351.16				1	9,853.81			
BU											
	<50	72,722	0.15	0.55	0.08	0.05	74,722	0.17	0.89	0.08	0.05
	50–100	1	57.60				12	66.91	10.37	65.52	
	100–200	2	138.43	34.09	138.42		5	148.19	32.89	144.35	
	200–500	1	230.67				1	447.92			
	500–1000						2	813.93	55.10	813.92	
SI											
	<50	1,474	0.21	1.29	0.01	0.01	855	0.33	1.51	0.03	0.01
	50–100	5	64.66	15.01	65.89		5	64.64	15.03	58.17	
	100–200	1	155.84				1	155.82			
	1000–10,000	3	2,275.18	1,062.9	2,869.89		3	2,284.28	1,073.0	2,609.68	
Total		387,954					318,068				

year. Higher number of patches in plantations with the smallest patch size indicates the forest plantations undertaken as gap-filling activities by the State Forest Department. Although the number of forest plantations with the smallest patch size decreased from 45,515 to 44,959 during 1975–2010, patches with moderate patch size (50–500 sq. km) increased from 6 to 10. Similar trend was observed in all other LULC classes, except water body and built-up land.

Highest mean patch size was observed in agricultural land, which decreased from 55,835.43 to 50,146.25 sq. km during 1975–2010; while the number of patches increased from 9 to 10 (Table 6), indicating expansion of agricultural land. Similarly, mean patch size in deciduous forests decreased from 24,222.78 to 21,322.36 sq. km during the study period, which could be attributed to forest loss due to degradation, deforestation and human interference in the forests sharing non-forest edge. Highest mean patch size in built-up land in 1975 was 230.67, which increased to 813.93 sq. km in 2010, which highlights intensive development in human settlements in the basin. The highest mean patch size in water body was 9351.16 sq. km in 1975, which increased to 9853.81 sq. km by 2010. This could be due to development of dams and canals in the basin during the last 35 years. The highest patch size in mixed forest (MF) also showed similar pattern with increase from 1833.71 to 2032.89 sq. km during 1975–2010. This could be attributed to 77 sq. km increase in MF during the period. The highest patch size in scrubland and wetland was 2002.1 and 316.22 sq. km in 1975, which reduced to 1890.02 and 288.78 sq. km by 2010 respectively. This could be due to conversion of 2993 sq. km of scrubland and 2310 sq. km of wetland to agricultural land during the period.

Understanding landscape dynamics in IGRB provides insights into the issue of rapid change in this region due to the 'green revolution', population explosion, industrial development and urbanization. Over expanding agricultural and built-up land pose a threat to the forest vegetation in the surrounding regions, as revealed by the study. The landscape dynamics in IGRB during 1975–2010 demonstrates a prominent increase in class area, particularly in agricultural land, built-up land and forest plantations; while there is a decrease in forests, mangroves, scrubland, wasteland and waterbody. The highest changes were observed in the built-up class, i.e. with 45.03% increment. Agricultural practices have rapidly grown in this region after the 'green revolution' in 1960s. Most of the forest cover has been converted to agriculture and built-up area. Rapid urbanization and industrialization are the main causes of expansion of settlement in the study area. The possible causes of increase in built-up land might be attributed to increase in population, urbanization, industrial development and economic development of the area. The increase in degraded forest, grasslands and mixed forests indicates degradation of forest. A general trend in the context of degradation of natural ecosystems has been observed in the study, which indicates conversion of dry deciduous forest and mixed forests to degraded forests, followed by conversion to scrubland/grassland and wasteland and finally take over of the land for the purpose of agricultural practices. Evergreen needle-leaved forest and evergreen broadleaved forest have experienced minimum change because these are the dominant ecosystems in western Himalayan forests and are less exposed to human interference as compared to deciduous forest.

The LULC classification scheme adopted here has proved to be useful, as it has captured the changes appropriately. On-screen visual interpretation-based LULC maps generated under the study for 1975 and 2010 are more than 85% accurate, which could be utilized as baseline maps for future studies on agriculture, hydrology, climate change and biodiversity. The landscape dynamics in IGRB demonstrates the present status of the river basins in other developing countries, which are facing various challenges due to natural and anthropogenic climate change. Agricultural lands covered the highest area (>70%), where low to medium-sized patches expanded and patches of higher size had slightly reduced in size over past decades. Thenkabail *et al.*[20] using MODIS datasets of 2001 and 2002, observed that approximately 60% of land cover in GRB is dominated by agricultural lands. Major change was observed with the expansion of agricultural lands and human settlements and depletion of forests. Moors *et al.*[21] project 90% growth in irrigated agriculture by 2020. Utility of visual interpretation technique and medium-resolution satellite imageries proved effective in capturing the built-up land that has shown the highest increase in percentage area. The increase of forest plantations is a positive sign in the basin, though degradation and loss of forest area was reported in terms of landscape indices. In general, the aggregation of agricultural patches and reduction of forest patches in small to medium sized patches was observed. We argue the utility of on-screen visual interpretation technique in favour of LULC mapping to achieve absolute accuracy in such a heterogeneous landscape like GRB, as it incorporates the interpreter's knowledge into the classification and mapping exercise. We appreciate the free availability of Landsat imageries having very good radiometry for scientific exercises that has substantially minimized the cost. We hope that the present study will provide insights in understanding landscape dynamics that could help in designing an effective land-use policy for the IGRB.

1. Turner, W., Spector, S., Gardiner, N., Fladeland, M., Sterling, E. and Steininger, M., Remote sensing for biodiversity science and conservation. *Trends Ecol. Evol.*, 2003, **18**, 306–314.
2. Shao, G. and Wu, J., On the accuracy of landscape pattern analysis using remote sensing data. *Landsc. Ecol.*, 2008, **23**, 505–511.
3. Gustafson, E. J., Quantifying landscape spatial pattern: what is the state of the art? *Ecosystems*, 1998, **1**, 143–156.
4. Wade, T. G., Riitters, K. H., Wickham, J. D. and Jones, K. B., Distribution and causes of global forest fragmentation. *Conserv. Ecol.*, 2003, **7**, 7.
5. Laurance, W. F., Sayer, J. and Cassman, K. G., Agricultural expansion and its impacts on tropical nature. *Trends Ecol. Evol.*, 2014, **29**, 107–116.
6. Lambin, E. F. and Meyfroidt, P., Global land use change, economic globalization, and the looming land scarcity. *Proc. Natl. Acad. Sci. USA*, 2011, **108**, 3465–3472.
7. Gilbert, N., Claims of growth in India's forests 'misleading'. *Nature*, 2010; doi:10.1038/news.2010.421.
8. Tang, J., Wang, L. and Yao, Z., Analyzing urban sprawl spatial fragmentation using multi-temporal satellite images. *GISci. Remote Sensing*, 2006, **43**, 218–232.
9. Olsen, L. M., Dale, V. H. and Foster, T., Landscape patterns as indicators of ecological change at Fort Benning, Georgia, USA. *Landsc. Urban Plann.*, 2006, **79**, 137–149.
10. Shi, X., Zhao, C., Wang, D. and Ouyang, W., Landscape dynamics analysis of guide wetlands in Yellow River watershed by Landsat series data. The International Archives of the Photogrammetry. *Remote Sensing Spatial Inf. Sci.*, 2008, **37**, 247–252.
11. Paudel, S. and Yuan, F., Assessing landscape changes and dynamics using patch analysis and GIS modeling. *Int. J. Appl. Earth Obs. Geoinf.*, 2012, **16**, 66–76.
12. Behera, M. D., Kushwaha, S. P. S. and Roy, P. S., Forest vegetation characterization and mapping using IRS-1C satellite images in Eastern Himalayan region. *Geocarto Int.*, 2001, **16**, 53–62.
13. Yuan, F., Sawaya, K. E., Loeffelholz, B. C. and Bauer, M. E., Land cover classification and change analysis of the Twin Cities (Minnesota) Metropolitan Area by multitemporal Landsat remote sensing. *Remote Sensing Environ.*, 2005, **98**, 317–328.

14. Lillesand, T. M., Kiefer, R. W. and Chipman, J. W., *Remote Sensing and Image Interpretation*, John Wiley, 2004, 5th edn.
15. Roy, P. S., Kaul, R. N., Sharma Roy, M. R. and Garbyal, S. S., Forest-type stratification and delineation of shifting cultivation areas in the eastern part of Arunachal Pradesh using LANDSAT MSS data. *Int. J. Remote Sensing*, 1985, **6**, 411–418.
16. Cadenasso, M. L., Pickett, S. T. and Schwarz, K., Spatial heterogeneity in urban ecosystems: reconceptualizing land cover and a framework for classification. *Front. Ecol. Environ.*, 2007, **5**, 80–88.
17. Chitale, V. S., Behera, M. D., Matin, S., Roy, P. S. and Sinha, V. K., Characterizing *Shorea robusta* communities in the part of Indian terai landscape. *J. For. Res.*, 2014, **25**, 1–8.
18. National Ganga River Basin Authority, *Environmental and Social Management Framework (ESMF), Volume I – Environmental and Social Analysis*, MoEF, GoI, 2011.
19. Singh, A. K., Probable agricultural biodiversity heritage sites in India: XI. The upper Gangetic Plains region. *Asian Agri-Hist.*, 2012, **16**, 21–44.
20. Thenkabail, P. S., Schull, M. and Turral, H., Ganges and Indus river basin land use/land cover (LULC) and irrigated area mapping using continuous streams of MODIS data. *Remote Sensing Environ.*, 2005, **95**, 317–341.
21. Moors, E. J., Groot, A., Biemans, H., van Scheltinga, C. T., Siderius, C., Stoffel, M. and Collins, D. N., Adaptation to changing water resources in the Ganges basin, northern India. *Environ. Sci. Policy*, 2011, **14**, 758–769.

ACKNOWLEDGEMENTS. We thank the Ministry of Environment and Forests, New Delhi for supporting the work through the 'Ganga River basin environmental management plan' project. The Landsat data gathered from Global Land Cover Facility (www.landcover.org), were utilized in this work. We also thank the two anonymous reviewers for their comments on the earlier version of the manuscript.

Received 4 April 2014; revised accepted 2 June 2014

Studies on remating behaviour in the *Drosophila bipectinata* species complex: evidence for sperm displacement

Akanksha Singh and Bashisth N. Singh*

Genetics Laboratory, Department of Zoology,
Banaras Hindu University, Varanasi 221 005, India

In *Drosophila bipectinata* female remating with respect to productivity and sperm displacement was studied by employing two mutant strains and a wild-type strain. The comparison of productivity between once-mated (control) and remated females revealed that the productivity of remated females is significantly higher than that of once-mated females in all the crosses showing increased productivity after remating. The P2′ values (proportion of second male progeny produced after remating) were calculated to test sperm displacement in each cross of remated females, which range from 0.60 to 0.67 extending the evidence for sperm displacement in *D. bipectinata*.

*For correspondence. (e-mail: bashisthsingh2004@rediffmail.com)

Keywords: *Drosophila bipectinata*, female remating, postcopulatory sexual selection, sperm displacement.

WHEN a female insect mates with multiple males their ejaculate may temporally overlap[1], generating intrasexual conflict between sexes over paternity[2], which is an indirect consequence of female remating, selection on male traits that enhance competitive fertilization success[3–5] and selection on female traits that mediate cryptic female choice[6,7]. These selective pressures collectively constitute postcopulatory sexual selection which generates variation in male and female behaviour[8]. Postcopulatory sexual selection includes both male–male competition (sperm competition) and female choice (cryptic female choice)[7] and plays a profound role in population divergence[9,10]. Traditionally, sperm competition has been seen as an intra-sexual conflict with the female being an inert arena in which the conflict occurs[9]. In the reproductive tract, females exert choice (cryptic female choice) on the sperm and select the most compatible sperm. However, sperm of the males compete among themselves for fertilizing the eggs and the one which is superior wins the battle. Thus both males and females play a role in the selection process.

The existence and relevance of sperm competition in *Drosophila* has been a contentious issue in evolutionary genetics[10]. The phenomenon of sperm competition occurs in many insect species, particularly in *Drosophila* females because of: (i) ability of females to store sperm from different males[11–14], (ii) the highly efficient use of stored sperm at fertilization[13,15], and (iii) the high probability of multiple mating[9]. After remating it has been observed that the sperm from the last (or second) male usually takes precedence over those of previous males and preferentially fertilizes subsequent eggs, a phenomenon known as sperm displacement or sperm precedence[16].

The study of sperm competition has centred around the question of whether females tend to remate only after most of the stored sperm has been utilized, i.e. sperm dependence of remating[14], or whether remating occurs relatively rapidly and before the first male sperm has been substantially depleted[5]. Most studies of postcopulatory sexual selection have focused on the pattern of sperm precedence, such as the proportion of progeny sired by the second male in a double mating trial (P2). The P2 value varies from 0 to 1. A P2 value of 0.5 is usually taken as evidence that the sperm of the two males are equally mixed in store. Whereas P2 value of 0 or 1 may indicate that the sperm of the first or second males has gained complete precedence over that of other males, or that sperm from the first or second male has become depleted or lost[9].